INSTITUTE OF PHYSICS PUBLISHING JOURNAL OF PHYSICS: CONDENSED MATTER

J. Phys.: Condens. Matter **18** (2006) 1–10 doi:10.1088/0953-8984/18/0/000

Short time investigation of the Neurospora-Kinesin step

Lorenzo Busoni, Aurélie Dupont, Clémentine Symonds, Jacques Prost and Giovanni Cappello

Institut Curie, CNRS UMR 168, Paris, 75248, France

E-mail: Giovanni.Cappello@Curie.fr

Received 9 November 2005
Published
Online at stacks.iop.org/JPhysCM/18/1

Abstract

The kinesin is a dimeric molecular motor, which processively moves along the microtubule in a sequence of 8 nm steps. The stepping dynamics needs to be clarified: there are controversial reports about the existence of substructures in the mechanical step and the step timescale. We present observations of the kinesin steps in the absence of external forces, measured with subnanometre precision and microsecond time resolution using a technique which we have recently introduced and named *travelling wave tracking*. The data suggest that, at zero load, the 8 nm step occurs in less than 30 μs and without any long mechanical substeps.

1. Introduction

The mechanism by which the kinesin–microtubule complex converts the chemical energy obtained from the ATP hydrolysis into mechanical work is becoming better and better understood. The genetic approach, together with an increasing amount of structural information, has established the relationship between the structure and the function of the kinesin [1, 2]. Complementarily, single molecule studies have supplied a detailed description of the kinesin–microtubule dynamics. Conventional kinesin is a dimer of two identical subunits, composed of two motor heads and a coiled-coil stalk. This two-headed motor moves processively [3] towards the plus-end of microtubules and can develop forces of a few piconewtons (stall force $\approx$ 6–7 pN). The motion is achieved by discrete steps of 8 nm [4–6], which correspond to the periodicity of the $\alpha\beta$-tubulin arrangement in microtubules.

In order to describe the physical mechanism of the kinesin step, two hypotheses have been proposed. In a pure mechanical model, a conformational change takes place during the chemical cycle and propels the trailing head forwards (toward the next binding site) while the leading head remains tightly attached to the microtubule. An alternative model is based on a thermal ratchet mechanism: the trailing head unbinds from the microtubule and, by thermal diffusion, randomly searches for the next binding site. Regimes combining both mechanisms are also possible.

To understand this mechanism, it is essential to provide a detailed description of the kinesin motion, such as the timescale of the step, its shape and any internal substructure [7, 8].

The existence of substructures within the 8 nm step is a controversial point: some works on the *drosophila kinesin* (kinesin-1) have reported the existence of mechanical substeps [9, 10] in the presence of an external load (force $>$ 1 pN). Conversely, other experiments performed in similar conditions showed that the step happens with no internal structure [11]. Additional information about the step features in the limit of zero force can help to confirm or infirm the existence of substeps. Q.4

In order to measure the step details in the absence of external force, we developed a technique for the tracking of particles with high spatial and temporal resolution: travelling wave tracking (TWT) [12]. This technique, described in section 2, permits the tracking of the motion of a kinesin without external manipulation and makes possible the measurements at zero force. The experiments are carried out in a classical bead assay configuration, with a 200 nm polystyrene particle, coated with kinesin and free to move along the microtubule. The bead position is recorded with subnanometre precision and a temporal resolution of 2 μs. As the spatial resolution is limited by the thermal fluctuations of the bead, we average over many steps in order to improve the signal to noise ratio. We thus can look for any internal structure within the 8 nm step, and provide bounds on the stepping timescale.

2. Travelling wave tracking

Conventional tracking techniques are based on spatially resolved detectors, and consist in measuring the light scattered from a relatively small probe, a small bead or fluorescent dye, moving in a uniformly illuminated field [13]. These techniques use charge-coupled devices (CCD cameras) or quadrant photodiode detections.

The travelling wave tracking (TWT) technique works in the opposite way: the scattered light is recorded by a point detector (Avalanche Photodiode—APD), with a broad bandwidth ($\sim$10 MHz), as the probe moves through a pattern of fringes. The fringes are obtained by interference of two laser beams with slightly different frequencies such that the pattern continuously shifts through the sample at constant speed. As a result, the sample is illuminated by a progressive sinusoidally modulated intensity

$$I(x,t) \propto 1 + \sin(qx - \Omega t), \tag{1}$$

where the fringe period d is $2\pi/q$ and the pattern shifts with a speed $v_f \equiv \Omega/q$ (in our setup $d \approx 200$ nm and $\Omega \approx 4$ MHz).

Let us imagine a small particle (a 100 nm polystyrene bead) immobile in the microscope: it scatters a light intensity proportional to $I(x,t)$ and hence *blinks* at frequency Ω. The APD records the light scattered from the bead, $I_{\mathrm{APD}} \propto 1 + \sin(\Omega t + \varphi)$, where the phase φ depends on the bead position in the fringes. If the bead moves over a distance δx from the position x' to $x' + \delta x$, the phase shift will change from φ' to $\varphi' + q \cdot \delta x$. In such a way, any displacement of the bead can be precisely determined, by measuring the phase shift $\varphi(t)$ as a function of time. In the following we will describe how the *travelling fringes* have been designed and the way to measure the phase shift.

The sinusoidal modulation is obtained by interference of two laser beams, with opposite wavevectors k_x, undergoing total internal reflection at the glass/water interface. In this setup, the fringe periodicity is 197 $\pm$ 2 nm. The light, totally reflected at the glass/water interface, does not penetrate into the sample and its intensity decreases exponentially with a characteristic penetration depth $\zeta \simeq 215$ nm. Figure 1 shows a schematic view of the experimental setup, as previously described [12].

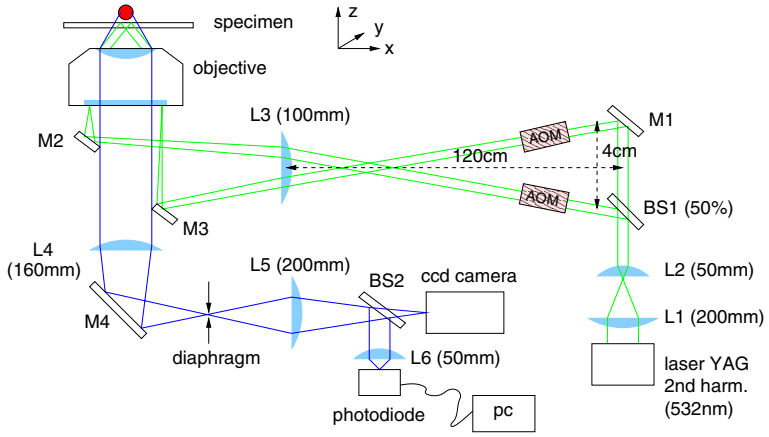

Figure 1. Scheme of the experimental setup. The *travelling wave tracking* configuration through the TIRF objective. The laser beam is compressed by means of a telescope (lenses L1 and L2) and split into two beams (beam splitter BS1) of equal intensity and polarization. The acousto-optic modulators (AOMs) shift the frequency of the laser beams, which are focused (lens L3) on the diameter of the back focal plane, in order to illuminate the sample with two parallel beams of opposite wavevector k_x. The scattered light is collected by the lenses L4, L5 and L6 and focused on the avalanche photodiode and/or on a CCD camera. M1, M2, M3 and M4 are mirrors and BS2 is a 1%–99% beam splitter.

(This figure is in colour only in the electronic version)

In order to obtain a travelling wave, we chose to slightly shift the frequency ω of both laser beams by $\Delta\omega_1$ and $\Delta\omega_2$ respectively. The frequency difference $\Omega = \Delta\omega_1 - \Delta\omega_2$ is set in such a way that the pattern moves much faster than any probe motion. The resulting intensity on the specimen can be written as: Q.5

$$I(x, z; t) = |\vec{E}_1 + \vec{E}_2|^2 = 2\mathbf{E}_0^2[1 + \cos(2kx - \Omega t)]\mathrm{e}^{-z/\zeta}. \tag{2}$$

The intensity $\mathcal{I}_{\mathrm{APD}}$, measured by the photodiode, is proportional to $I(x, z; t)$ (equation (2)): the resulting signal is a sine-like modulation, whose amplitude and phase depend respectively on the z and the x position of the probe. Both the phase $\varphi(t)$ and the amplitude $A(t)$ are extracted by using a lock-in amplifier with a 300 kHz bandwidth and they are recorded with a sampling rate of 625 s^{-1}. The two coordinates $x(t)$ and $z(t)$ are:

$$\begin{aligned} x(t) &= \frac{d}{2\pi}\varphi(t) \\ z(t) &= z_0 - \zeta \ln A(t). \end{aligned} \tag{3}$$

z_0 is unknown, which implies that we do not measure the absolute z position of the probe.

The resolution and the performances of this setup have been characterized using a piezoelectric stage, which moves a bead stuck to the coverglass by steps of 10 nm. As explained above, this motion induces a phase shift $\varphi(t)$, which we measure. Figure 2(A) shows how $\varphi(t)$ (right axis on the plot) evolves as a function of time, proportionally to the bead position (left axis). The 10 nm displacements are easily observed and the internal structure of the step can be characterized with nanometre precision. The oscillatory motion after the step is due to the inertial behaviour of the piezoelectric stage: without any feedback loop, it oscillates with exponentially damped amplitude after step-like impulses. The intrinsic noise of the experimental setup can be measured by analysing the parts of the curve where the oscillations are completely damped (see figure 2, inset). The plot shows that the intrinsic noise is 3 Å RMS; this noise is *white* and totally uncorrelated, and it is due the residual shot noise.

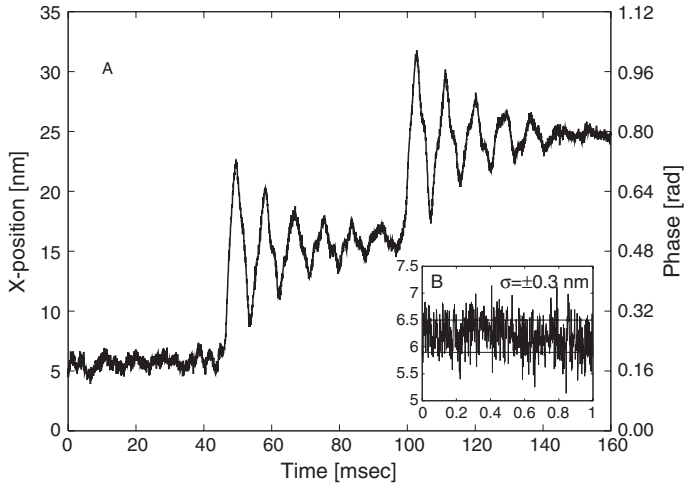

Figure 2. A single colloid (diameter 200 nm) is fixed on the coverglass, while the sample holder is moved in 10 nm steps by means of a calibrated piezoelectric stage. Inset: the residual shot noise limits the resolution to 3 Å RMS.

3. Methods

Nkin460GST is expressed in BL21 (DE3) *E. coli* and purified as described in [14, 15].

Preparation of the microtubules. The microtubules are polymerized at a concentration of 2 mg ml^{-1} (concentration adjusted with BRB80: 80 mM K-PIPES pH 6.9, 1 mM $MgCl_2$, 1 mM EGTA, 1 mM GTP) and at a temperature of 37 °C for 30 min. Then, in order to stop the polymerization/depolymerization process, taxol is added at a final concentration of 20 μM and the solution is stored at 37 °C for 5 min. Unpolymerized tubulin is removed by centrifugation at 30 000 RPM, during 15 min at 30 °C. The pellet is rinsed and resuspended with BRB80 supplemented with 10 μM taxol) . Q.6

Bead assay. Microtubules are introduced in a flow chamber and incubated for 3 min to adsorb on a poly-L-lysine-coated coverglass. The chamber is rinsed with BRB80+taxol and with filtered casein solution (2 mg ml^{-1}) to avoid nonspecific interaction. After a last wash with BRB80, the kinesin-coated beads are mixed with the motility buffer and injected into the chamber. Kinesin-coated beads are prepared by mixing a highly diluted preparation of kinesins and carboxylated latex beads (200 nm diameter; Polysciences cat 07304). After incubating for Q.7 5–10 min, filtered casein at 1 mg ml^{-1} is added to this mixture. The motility buffer is a BRB80 buffer supplemented with 20 μM ATP, 1 mM phosphocreatine, 50 μg ml^{-1} creatine phosphokinase and an oxygen scavenging system (3 mg ml^{-1} glucose, 100 μg ml^{-1} glucose oxidase and 20 μg ml^{-1} catalase), 2 mM DTT. The coverslip is sealed with VALAP (vaselin, lanolin, Q.8 paraffin at 1:1:1). Observations are performed at room temperature (approximately 25 °C). Q.9

4. Results

When the microtubules are injected into the observation chamber, most of them are partially aligned by the flow. We take advantage of this effect to roughly line them up, perpendicularly to the interference fringes. The kinesin-coated beads come randomly in touch with the microtubules and move along them through the *travelling fringes*.

In vitro and at saturating ATP concentration ([ATP] = 10 mM) the N-kinesin moves faster than 2 μm s^{-1} [16]. In our experiments, the ATP concentration is tuned to slow the kinesin down to a speed which allows us to easily distinguish the steps. In general we used [ATP] $\leqslant$ 20 μM. The best way to know the number of motors pulling the bead is to measure the stall force, like in optical tweezers experiments. As in our setup we do not apply any external

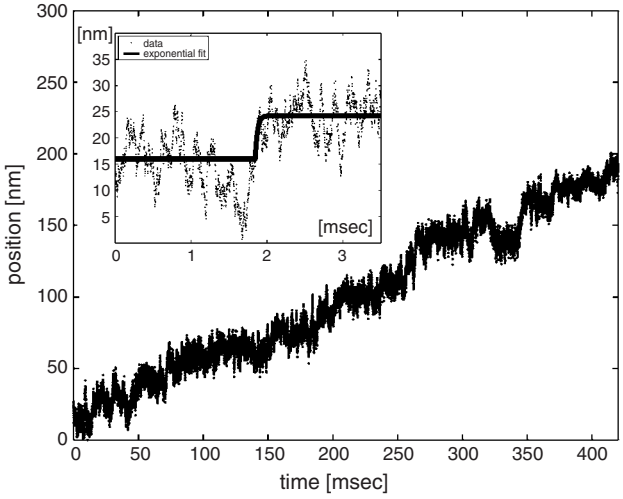

Figure 3. Kinesin-coated bead position as a function of time. Notice the discontinuities in the position, corresponding to the kinesin 8 nm steps. The data are acquired with full bandwidth. Inset: one single 8 nm step.

force, we cannot use this strategy. In order to get one single enzyme on the bead, we decrease the kinesin concentration down to the threshold where no events are observed. During the experiments, the kinesin concentration is set slightly above this threshold. By using an *ex situ* optical tweezers setup, we verified that, at this concentration, the stall force never exceeds a few piconewtons.

Figure 3 shows a record of kinesin motion: the plot shows the displacement (in nanometres) as a function of time (milliseconds), recorded with full bandwidth. We observe one of the most peculiar feature of kinesin: the motor moves along the microtubule by steps of 8 nm, which correspond to the microtubule periodicity. The inset of figure 3 shows a single 8 nm step with full bandwidth (time resolution of 2 μs).

As explained previously, we are interested in characterizing the kinematical features of the kinesin steps. From figure 3 it appears that the experimental noise is too high, in the full bandwidth track, to measure the step. In section 2 we have stated that the TWT resolution allows us to localize a bead stuck to the coverslip with a precision of ± 3 Å, which is roughly 15 times lower than the noise measured with the kinesin. The experimental noise is dominated by the Brownian motion of the bead, which thermally fluctuates around the kinesin position.

These observations raise two questions. First, how is it possible to extract information from this noise, in order to describe the dynamical properties of the kinesin-bead link. The second point is to understand how we can extract the kinesin step features from such a noisy signal. These questions are addressed in the following section.

5. Analysis and discussion

5.1. Thermal fluctuations

In our experiments, we measure the position $x_b(t)$ of a tethered bead pulled by a molecular motor (figure 3). As previously mentioned, the bead is not stiffly attached to the kinesin and it thermally fluctuates around the kinesin position $x_m(t)$. The kinesin–bead link acts as an attractive potential $U(x_b - x_m)$, which depends on the distance between the motor and the bead. Far from the kinesin steps, the energy released during the step by the ATP hydrolysis is completely dissipated and the fluctuations are only thermally excited (we will see in the following that the system relaxes with a time constant of $\tau \simeq 30$ μs). At thermal equilibrium,

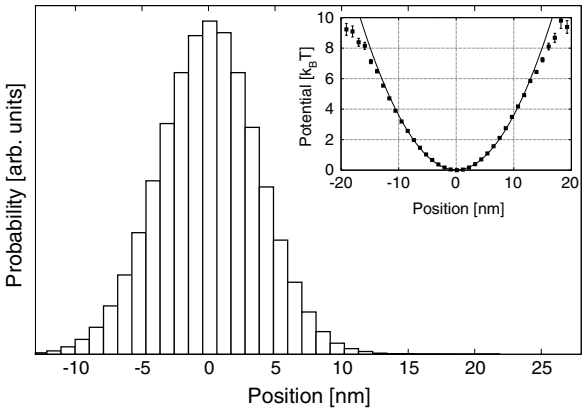

Figure 4. Probability distribution of the lateral distance bead–motor $x_b - x_m$. The bead–motor interaction potential is calculated by using the Boltzmann distribution.

the Boltzmann law gives the probability $P(x_b - x_m)$ of finding the bead at position x_b in the potential $U(x_b - x_m)$:

$$P(x_b - x_m) \propto e^{-U(x_b - x_m)/k_B T}. \tag{4}$$

Within the ergodic hypothesis, the Boltzmann equation allows us to estimate the potential of the bead–motor linkage:

$$U(x_b - x_m) = -k_B T \ln P(x_b - x_m) + \text{const.} \tag{5}$$

Experimentally, the probability $P(x_b - x_m)$ of finding the bead at a certain distance from the motor position is calculated for 70 plateaus between steps, corresponding to a total acquisition time of 0.8 s. As x_m is not directly measured, we assume that far from the steps the motor does not move and its position corresponds to the mean position of the bead ($x_m = \langle x_b \rangle$). Figure 4 shows the distribution $P(x_b - x_m)$ and the corresponding potential (figure 4, inset): we observe that the bead-motor interaction can be quite well approximated by a harmonic potential:

$$U(x_b - x_m) = \frac{\kappa_x}{2}(x_b - x_m)^2. \tag{6}$$

The continuous line is the best fit between the data and equation (6). This observation is in contrast with previous results, based on the optical tweezers technique, that pointed out a nonlinear behaviour of the kinesin–bead linkage when the kinesin tail is strongly elongated. The discrepancy can be understood if one takes into account the fact that, in our experiments, the bead explores only the bottom part of the potential, which is accessible by thermal fluctuations.

All the forces acting on the bead are known and the motion equation of the bead can be described by the Langevin equation:

$$\xi \dot{x}_b(t) + \kappa_x [x_b(t) - x_m] = \eta(t) \tag{7}$$

where ξ is the viscous drag and $\eta(t)$ the Brownian force. This equation can be analytically solved and the autocorrelation function $\Phi_x(\tau)$ of the bead position $x_b(t)$ becomes

$$\Phi_x(\tau) = \langle x_b(t) x_b(t+\tau) \rangle = \frac{k_B T}{\kappa_x} e^{-(\kappa_x/\xi)\tau} + \Lambda_x \delta(\tau) \tag{8}$$

where $\Lambda_x = 2.5$ nm^2 accounts for the amplitude of the *intrinsic*, uncorrelated, experimental noise. This term includes the shot noise and the uncertainty associated to the analogue/digital conversion of the signal, as well as all the other high frequency noises. The square amplitude of the thermal fluctuations is inversely proportional to the stiffness κ_x of the bead–kinesin linkage. Such thermally excited fluctuations, relax exponentially with a time constant $\tau_x = \xi/\kappa_x$. **Q.10**

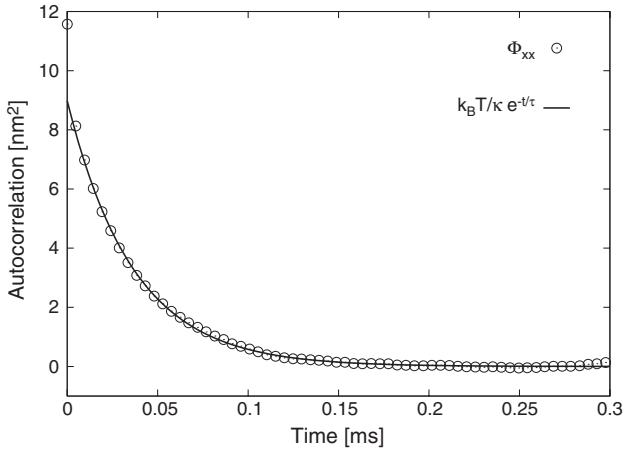

Figure 5. Position–position autocorrelation function of the bead, corresponding to Brownian fluctuations: $\Phi_x(\tau) = \langle x(t)x(t+\tau)\rangle$. The continuous line is the best fit according to equation (8).

The autocorrelation function $\Phi_x(\tau)$ is extracted from the experimental data and plotted in figure 5(a); the data (○) are fitted to equation (8) (continuous line). We first observe that the intrinsic noise is small compared to the thermal fluctuations ($\Lambda_x < k_B T/\kappa_x$). The fit yields $\kappa_x = 4.4 \times 10^{-4}$ N m^{-1} and $\tau_x = 36$ μs, where τ_x is the time needed by the system to relax to thermodynamical equilibrium. This time depends, of course, on the load and should be shorter for smaller cargos. For our 200 nm bead, the relaxation time τ_x appears to be very short compared to the ATP-ase cycle, which takes at least a few milliseconds. This means that after each step, the bead–kinesin system has the time to thermalize and the memory of each step is lost before the next step. Therefore, all the steps can be considered thermodynamically independent. **Q.11**

From the values of κ_x and τ_x we can estimate the local friction $\xi = 1.44 \times 10^{-8}$ N s m^{-1}. Within the hypothesis that the source of the friction was only the viscous drag of the bead, the expected value for a free 200 nm bead moving in the water would be $6\pi\eta R = 1.9 \times 10^{-9}$ N s m^{-1}, i.e. more than seven times smaller than the measured one. Such a high friction can be understood by taking into account the vicinity of the coverslip. Faucheux *et al* [17, 18] demonstrated experimentally that the diffusion coefficient is strongly reduced in a confined environment. A bead free to move close to a wall diffuses up to three time more slowly than the same bead in the same fluid. In our case, where the bead is not even free to rotate, the diffusion coefficient decreases as a logarithmic function of the bead–wall distance [19]. **Q.12**

In section 2 we have shown the possibility of tracking the particle simultaneously parallel and perpendicularly to the substrate, i.e. in this case respectively parallel and perpendicular to the kinesin motion. In order to characterize the perpendicular $z_b(t)$ motion we proceed as for the $x_b(t)$ analysis. The autocorrelation Φ_z follows equation (8) (x being replaced by z) and the best fit is obtained for $\kappa_z = 4.3 \times 10^{-4}$ N m^{-1} and $\tau_z = \xi/\kappa_z = 64$ μs. This result indicates that the stiffness of the kinesin–bead bond is essentially the same along the two directions, in the absence of external forces. In addition, the diffusion coefficient is reduced by a factor of 1.8 in the direction perpendicular to the surface. The coefficient Λ_z (uncorrelated noise) is larger than $k_B T/\kappa_z$ (the fit yields $\Lambda_z = 63$ nm^2 and $k_B T/\kappa_z = 9.5$ nm^2), which means that the experimental accuracy is $\simeq$5 times better in the x direction than along z. This is certainly due to the absence of lock-in detection along the z-direction: all the low frequency noises (laser instability and detection noises) are integrated.

5.2. Kinesin step analysis

As explained in the introduction, the aim of this work is to investigate the kinesin step, in order to determine the time necessary to move over the eight nanometres and to look for any possible fine structure of the step. The plot in figure 3 reveals an extremely unfavourable signal/noise ratio: any step detail is hidden by the noise, whose amplitude is comparable to the step itself. The extraction of the general features of the step is thus difficult. In the previous section we have identified in detail the origin of this noise, the main source of which is thermal. The autocorrelation analysis also indicates that the thermal fluctuations relax with time constant $\tau_x \sim 36\ \mu$s. This suggest a way to extract information about the kinesin step: select a sequence of N consecutive steps and average them; as the time lapse between steps is $\gg 36\ \mu$s, the thermal noise is completely uncorrelated from one step to the next. By averaging N steps, the noise decreases like $1/\sqrt{N}$ while the signal which adds coherently survives.

This averaging process is meaningful only to the extent that the steps are properly synchronized. As the step beginning t_i is unknown *a priori*, we first choose a trivial function, corresponding to the trajectory of the bead subsequent to an instantaneous motor step:

$$\tilde{\sigma}_{\mathrm{Fit}}(t) = a_i \vartheta(t) \mathrm{e}^{-t/\tau} + c_i, \tag{9}$$

where τ is fixed by time response of the bead, a_i is the step size, $\bar{t_i}$ is the starting time and $\vartheta(t)$ the Heaviside function. a_i and c_i are determined by fitting the position of the bead, respectively after and before the step. Then t_i is adjusted, by minimizing the sum

$$\int [x(t - t_i) - \sigma(t)]^2 \, \mathrm{d}x \tag{10}$$

with respect to t_i. With this procedure the synchronization uncertainty is

$$\delta t = \alpha \sqrt{\frac{k_{\mathrm{B}} T}{\kappa_x \ell^2}} \tau, \tag{11}$$

where $\ell = 8$ nm, and $\alpha \simeq 1$ and weakly depends on the guess function $\sigma(t)$. The choice of the guess function (equation (9)) is motivated by its simplicity. Different guess functions, which take into account more complex motor trajectory (i.e. the kinesin makes the step at constant speed or in an exponential manner), give very similar results. In our case $\delta t \simeq 20\ \mu$s.

We have averaged the data over 68 chosen among the best experimental sequences **Q.13** (figure 6, empty circles, ○). Data biased because of microtubule misalignment or suspicion of multiple attachments are discarded. In agreement with previous works, the average step amplitude is 8.0 ± 0.2 nm. We also observe that the bead approaches the final position in $\sim 30\ \mu$s with an exponential behaviour. This timescale is compatible with the exponential decay measured in the autocorrelation analysis (figure 5), and corresponds to the relaxation time response of the bead moving in a viscous environment. Even if the motor moved suddenly, the bead would follow with this delay, imposed by the local friction and the stiffness of the kinesin–bead linkage.

We do not observe, at this timescale and within our experimental resolution, any evidence for substeps, slow conformational change or any other fine structure in the step.

We also see that, in the limit of weak thermal fluctuations ($\eta(t) \ll 1$), equation (7) becomes

$$x_{\mathrm{m}}(t) = x_{\mathrm{b}}(t) + \tau_x \dot{x}_{\mathrm{b}}(t) \tag{12}$$

where τ_x is determined by the autocorrelation analysis (equation (8)). Thus, the motor position x_{m} can be directly deduced from the bead position x_{b} (figure 6, triangles, ▲).

The experimental data indicate a step time $t_{\mathrm{s}} \simeq 20\ \mu$s, shorter than the thermal fluctuation timescale. Obviously, the resolution is mainly limited by our synchronization procedure, which

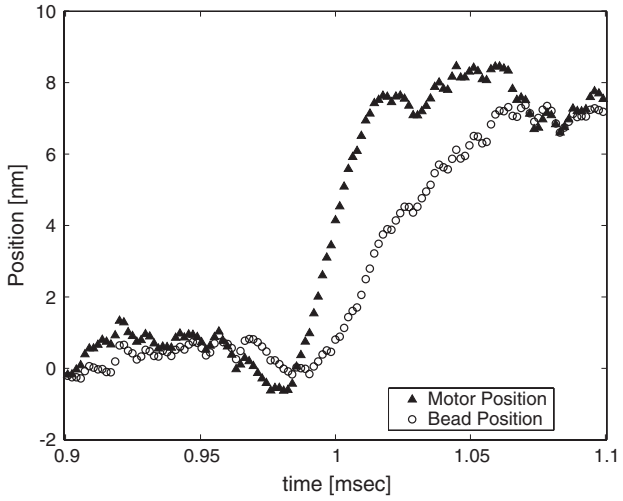

Figure 6. The average bead position x_b (○) during the 8 nm step: for each step, the starting positions t_i have been determined by a least-square fit to an exponential step. The motor position x_m (▲) is deduced from equation (12). This curve shows a rising time shorter than 20 μs.

introduces a broadening of the kinesin step (equation (11)) and, therefore, the kinesin moves even faster.

Such a short step-time is compatible with a simple free diffusion of the rear kinesin head, moving over a distance of 16 nm to reach the next binding site. If we consider the kinesin head like a 5 nm globular object [20] free to diffuse in the water, we can estimate the mean diffusion time over the next binding site:

$$t = \frac{\Delta x^2}{2D} = \frac{6\pi\eta R}{2k_B T} \times (16\ \text{nm})^2 \simeq 1.5\ \mu\text{s}. \tag{13}$$

We have seen in the previous section that the diffusion coefficient of the bead moving close to the microtubule should be corrected by a factor of 7. If we use the same correction for the kinesin head diffusion, we estimate an average diffusion time of $\simeq$10 μs, which is compatible with the measured value.

Conversely, assuming that 100% of the energy released by the ATP hydrolysis is converted into mechanical work and totally dissipated by hydrodynamical friction during the step, the speed time t would be

$$t = \frac{\Delta x}{v_m} = \frac{6\pi\eta R \cdot (\Delta x)^2}{E_{\text{ATP}\rightarrow\text{ADP+Pi}}} \simeq 1\ \mu\text{s}. \tag{14}$$

Of course, this assumption is quite optimistic, and the step time would be longer if only a part of the energy is directly used to move the trailing head forward. Eventually, this shows that both pure diffusion of the head and a power stroke mechanism would allow the kinesin to reach the next binding site more quickly than about 10 μs.

The experimental noise does not allow us to discriminate between different stepping models, such as smooth gliding of the motor head at constant speed, sudden jump or exponential approach to the next binding site. Nevertheless, our results supply an upper limit to the step timescale and definitely exclude any slow conformational change associated to the kinesin motion at zero force, and they do not indicate any evidence for sub-8 nm steps for Neurospora kinesin. These results are consistent with those observed under load by Carter *et al* [11]. They

are compatible with motion in which all chemical steps happen without detectable motion at subnanometre resolution and the one involving the chemo-mechanical coupling takes place on a microsecond timescale ($t \ll 30\ \mu$s).

6. Conclusion

We have presented a study of the fast conformational change of the Neurospora Crassa Kinesin. This molecular motor has been investigated using a simple and versatile tracking technique, travelling wave tracking, which allows us to measure the particle position with the precision of a few angstroms and a time resolution of 2 μs. Q.14

This technique is used to characterize the motion of the Neurospora-Kinesin in a bead assay, in the absence of external forces. The typical kinesin motion, with discrete 8 nm steps and relatively long dwell times, is observed. At the same time, the Brownian motion of the bead, around the kinesin position, is recorded in two dimensions: along and perpendicularly to the microtubule respectively. The kinesin–bead link is characterized and its stiffness is measured independently along both directions.

As the thermal fluctuations of the bead hide the short-time details of the steps, the signal/noise ratio has been improved by averaging many steps: we developed a simple algorithm to synchronize the steps and average over many events. The final temporal resolution is mainly limited by the bead response time, which is measured to be 30 μs.

Our results show that the kinesin stepping time is shorter than 30 μs, and that at this timescale no structure in the step is observed. The experiment results exclude any motion resulting from a slow conformational change and any mechanical substep longer than 30 μs.

Acknowledgments

We thank M Schliwa and R Cross for providing kinesins plasmid from *Neurospora Crassa*. This work was supported by grants from the EU (BIOMACH project).

References

[1] Endow S A and Higuchi H 2000 *Nature* **406** 913
[2] Bathe F, Hahlen K, Dombi R, Driller L, Schliwa M and Woehlke G 2005 *Mol. Biol. Cell* **16** 3529
[3] Inoue Y, Iwane A H, Miyai T, Muto E and Yanagida T 2001 *Biophys. J.* **81** 2838
[4] Svoboda K, Schmidt C F, Schnapp B J and Block S M 1993 *Nature* **365** 721
[5] Higuchi H, Muto E, Inoue Y and Yanagida T 1997 *Proc. Natl Acad. Sci. USA* **94** 4395
[6] Nishiyama M, Higuchi H and Yanagida T 2002 *Nat. Cell Biol.* **4** 790
[7] Visscher K, Schnitzer M J and Block S M 1999 *Nature* **400** 184
[8] Yildiz A, Tomishige M, Vale R D and Selvin P R 2004 *Science* **303** 676
[9] Coppin C M, Finer J T, Spudich J A and Vale R D 1996 *Proc. Natl Acad. Sci. USA* **93** 1913
[10] Nishiyama M, Muto E, Inoue Y, Yanagida T and Higuchi H 2001 *Nat. Cell Biol.* **3** 425
[11] Carter N J and Cross R A 2005 *Nature* **435** 308
[12] Busoni L, Dornier A, Viovy J-L, Prost J and Cappello G 2005 *J. Appl. Phys.* **98** 064302
[13] Yildiz A, Forkey J N, McKinney S A, Ha T, Goldman Y E and Selvin P R 2003 *Science* **300** 2061
[14] Crevel I, Carter N, Schliwa M and Cross R 1999 *EMBO J.* **18** 5863
[15] Lakamper S, Kallipolitou A, Woehlke G, Schliwa M and Meyhofer E 2003 *Biophys J.* **84** 1833
[16] Steinberg G and Schliwa M 1996 *J. Biol. Chem.* **271** 7516
[17] Brenner H 1961 *Chem. Eng. Sci.* **16** 242
[18] Faucheux L P and Libchabert A J 1994 *Phys. Rev.* E **49** 5158
[19] Goldman A J, Cox R G and Brenner H 1967 *Chem. Eng. Sci.* **22** 627
[20] Hirokawa N, Pfister K K, Yorifuji H, Wagner M C, Brady S T and Bloom G S 1989 *Cell* **56** 867